Surface Chemistry

DOI: 10.1002/anie.200800406

Surface Chemistry of Ag Particles: Identification of Oxide Species by Aberration-Corrected TEM and by DFT Calculations**

Dang Sheng Su, Timo Jacob, Thomas W. Hansen, Di Wang, Robert Schlögl, Bert Freitag, and Stephan Kujawa*

In the 1990s, by means of spectroscopic methods, Ertl et al. found surface and subsurface oxygen atoms on and in Ag catalysts.[1,2] Three species of atomic oxygen with distinct structural and energetic properties were identified. According to their TDS behavior (TDS: thermal desorption spectroscopy), a surface atomic species was termed the α form, and a bulk-dissolved species of lower interaction energy the β form. Finally, γ-oxygen was identified as strongly interacting atomic oxygen with high electron density, incorporated into the top atomic surface layer of Ag.[3] As silver catalysts are used in many reactions, for example, hydrogenation of unsaturated aldehydes,[4] partial oxidation of methanol to formaldehyde,[1] and oxidative coupling of methane to ethane and ethylene,[2] the discovery of surface and subsurface oxygen atoms in Ag is of great significance for understanding the catalytic reaction steps and mechanisms of silver catalysts. However, the location of surface and subsurface oxygen atoms remains an unanswered question in Ag catalysis and, perhaps more importantly, it is unclear whether nonmodel industrial catalysts exhibit the same surface chemistry.

High-resolution transmission electron microscopy (HRTEM) has been widely used to study the morphology and structure of catalysts. It provides detailed information on the micro- and nanostructure of catalysts.[5,6] By aligning the normal of a given surface perpendicular to the incident electron beam,[7,8] the surface structure and its relationship to the underlying bulk structure can be investigated. However, due to the artefacts caused by spherical aberration of magnetic imaging lenses, conventional TEM is not optimally suited to obtaining readily interpretable images of catalyst surfaces. One major artefact is the delocalization of image details, which appears as an extension of the perimeter of a sample beyond the actual surface. In this study, we investigated an Ag/SiO_2 catalyst using a TEM with a spherical-aberration corrector that can compensate for these problems and thus provide detailed information about the structure of the surfaces of a silver-based catalyst. With the support of DFT calculations, the positions of α- and γ-oxygen on the surfaces of Ag particles have been determined for the first time. Furthermore, the presence of local surface oxygen atoms or oxide was verified.

To investigate Ag particles by a direct imaging technique, spatial frequencies in the band between 4.24 and 4.89 nm^{-1} representing Ag(111) and Ag(200) lattice-plane distances of 0.236 and 0.204 nm, respectively, must be transferred with the same contrast. Under the experimental conditions shown in Figure 1 the acquired high-resolution electron micrograph makes the surface terminations of the Ag particle clearly observable (Figure S1 and Figure 2). The internal crystalline structure of the Ag particles extends to the surface, where it is terminated abruptly in different ways. Steps consisting of one or two atom rows on the (111) facet are observed.

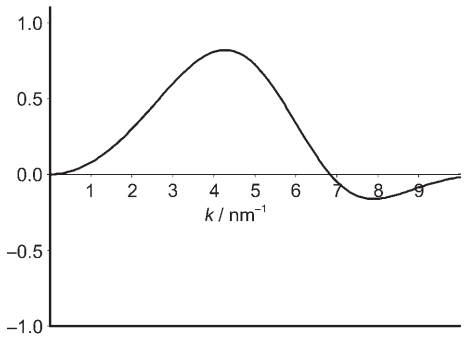

Figure 1. Contrast transfer function of the 200-kV FEG (field emission gun) aberration-corrected TEM with which the high-resolution images were taken. A defocus (δf) of two Scherzer ($\delta f = 2(C_s\lambda) - 1/2 \approx 10$ nm) was chosen in order to optimize the main transfer band to the spatial frequency (k) band of interest.

High-resolution images reveal that, if the surface is terminated abruptly with a (111) facet, no changes in lattice spacing of the (111) planes or surface reconstruction is observed. However, modification of the surface structure within the (111) planes is observed. Figure 2 shows a high-resolution (HR) TEM image of a silver particle with the [110] zone axis parallel to the primary electron beam. In this orientation, atomic columns can be considered to be aligned within the $(1\bar{1}1)$ planes (parallel to the surface), and within

[*] Dr. D. S. Su, Dr. T. Jacob, Dr. T. W. Hansen, Dr. D. Wang, Prof. R. Schlögl
Fritz-Haber-Institut der Max-Planck-Gesellschaft
Faradayweg 4–6, 14195 Berlin (Germany)
Fax: (+49) 30-8413-4401
E-mail: dangsheng@fhi-berlin.mpg.de
Dr. B. Freitag, Dr. S. Kujawa
FEI Europe, Achtseweg Noord 5 Bldg.
5651 GG Eindhoven (The Netherlands)

[**] The work in Berlin is part of the EnerChem project of the Max-Planck-Gesellschaft. T.J. gratefully acknowledges support by the "Fonds der Chemischen Industrie" and the "Deutsche Forschungsgemeinschaft (DFG)" within the Emmy-Noether Program. The authors thank Prof. Claus, TU Darmstadt, for providing the samples which were prepared within the "Brückenschlag" Project of the DFG.

Supporting information for this article is available on the WWW under http://www.angewandte.org or from the author.

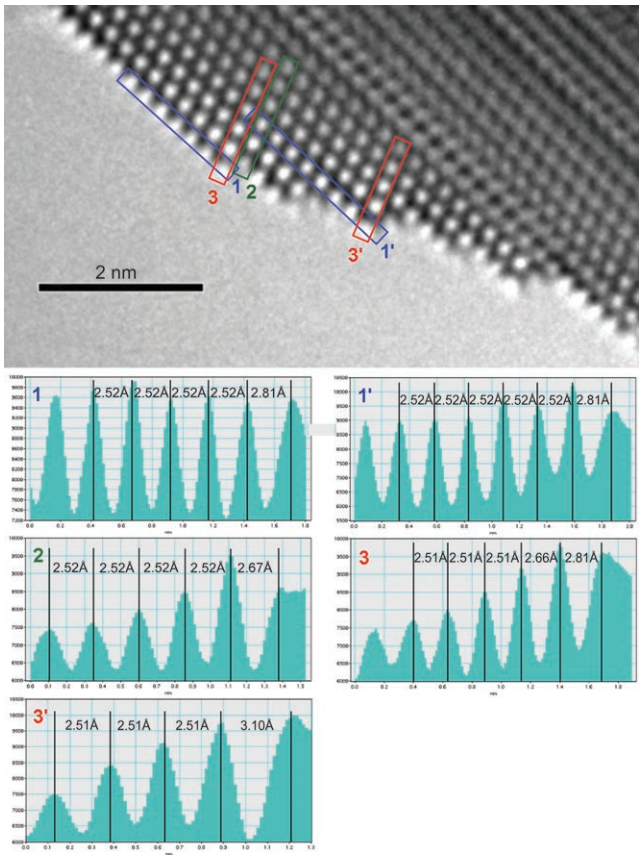

Figure 2. HR image of an Ag particle surface in the [110] projection, with intercolumn distance analysis along line profiles 1 and 1′ in $(1\bar{1}1)$ surface planes, line profile 2 in a $(\bar{1}11)$ plane terminating directly below the step, and line profiles 3 and 3′ in $(\bar{1}11)$ planes terminating directly at the step edge.

the $(\bar{1}11)$ planes, with a mutual angle of 70.53°. Intensity profiles within the $(1\bar{1}1)$ and $(\bar{1}11)$ planes corresponding to the lines indicated on the image are also shown. For perfect Ag crystals, the intercolumn distance in the {111} plane is 2.53 Å. From line profiles 1 and 1′ in Figure 2, the distance between the two outermost atom columns in the terminating $(1\bar{1}1)$ plane is about 2.80 Å, significantly larger than the intercolumn distance in the bulk. Similarly, an intercolumn expansion of the same order of magnitude is observed at the step-edge termination along the $(\bar{1}11)$ planes inclined 70.53° to the $(1\bar{1}1)$ surface, labeled as line profiles 3 and 3′ in Figure 2. Such an expansion is less significant along line profile 2 terminating directly below the step.

On a clean metal surface, the outermost surface atoms are expected to be pulled towards the bulk due to the missing coordination outside the surface. Especially the Ag atoms at the edge of a terrace are expected to be more strongly bound to the bulk. This is confirmed by DFT calculations of the Ag surface structure (see below). However, expansion of the surface layer towards the vacuum was observed in Figure 2. To illustrate this point, the silver surface is compared with a gold particle surface in Figure S2. The expected movement of the outermost gold atom towards the bulk is seen, contrary to the observation for the Ag particle.

DFT calculations were performed on (100) steps of Ag with and without adsorption of oxygen. On the clean step edges the step length was first varied. The surface Gibbs energy was found to decrease from 0.058 eV Å^{-2} for a two-atom-wide step to the asymptotic value of 0.051 eV Å^{-2} corresponding to an infinitely extended Ag(111) surface. In contrast, the interatomic distance shows only minor variation with step length, and thus is comparable to the distances summarized in Table 1. Since atom Ag3 (see Figure 3 d), which is located directly at the step edge, has a lower coordination number than the other surface atoms or the bulk atoms, it moves slightly into the step during geometry optimization. Therefore, along directions 1 and 3 (see Figure 2) the projected atom spacing near the step edge is slightly decreased compared to the value of the perfect Ag(111) surface or bulk Ag of 2.533 Å. Due to this reduced bond length of Ag3, Ag2, located directly below the step, moves slightly into the vacuum by about 0.04 Å. In contrast to the calculated inward shift of Ag3, the analysis of the TEM images showed that on a substantial number of (100) steps Ag3 is shifted outwards with an increase in projected atom spacing of about 0.3 Å.

Table 1: Projected interatomic distances before and after adsorption of oxygen on a four-atom-wide (100) step. The directions are as indicated in Figure 3 c with the indices on the distances starting with the Ag atom at the (100) step.

Direction	System	d_{12} [Å]	d_{23} [Å]	d_{34} [Å]	d_{45} [Å]
1	clean step	2.499	2.507	2.514	2.544
	with 1 O atom	2.380	2.401	2.414	2.736
	with 2 O atoms	2.761	2.394	2.408	2.587
2	clean step	2.571	2.528	2.518	2.527
	with 1 O atom	2.547	2.511	2.511	2.517
	with 2 O atoms	2.453	2.483	2.505	2.513
3	clean step	2.451	2.518	2.533	2.536
	with 1 O atom	2.773	2.502	2.530	2.531
	with 2 O atoms	2.770	2.529	2.561	2.543

To address this discrepancy, DFT calculations were performed with oxygen adsorbed at different positions of a four-atom-wide (100) step by using a (4×1) unit cell. For the resulting oxygen rows various surface and subsurface positions (Figure 3 a) were studied. The corresponding binding energies are summarized in Table 2. Focusing first on the on-surface positions, it was found that a single oxygen atom per step-edge atom preferentially binds below the step edge (position C) or at position B, mimicking the Ag(111) terrace. Binding on top of the step edge (position A) is about 0.54 eV less stable. However, the overall preferred binding site is position E, that is, in the (100) microfacet of the step. Since this microfacet is more open than the close-packed (111) surface, oxygen diffuses into the step and forms a local oxide at the (100) step. Due to the presence of this oxygen, Ag3 is pushed outwards, and this leads to a projected spacing to the next atom along direction 3 (Ag4) of 2.773 Å, which is in good agreement with the value obtained from the TEM analysis. However, along direction 1 the presence of a single oxygen atom per step edge causes a contraction, which is in contra-

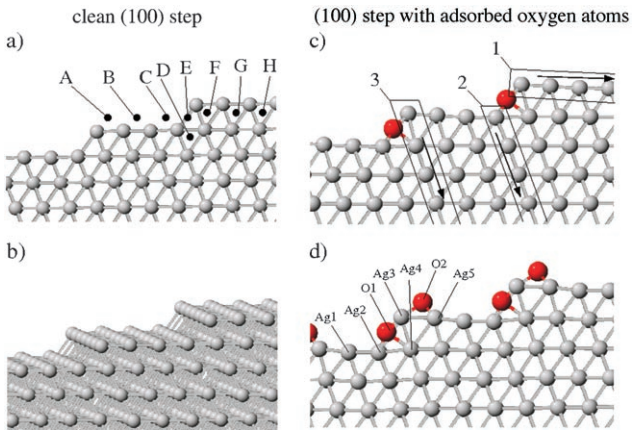

Figure 3. Optimized structures before (left) and after adsorption of oxygen (right), see text for details. The labels in (a) indicate the various positions at which oxygen adsorption was calculated. The numbered boxes in (c) give the directions for which the projected atom spacing, counted along the arrows, is summarized in Table 1.

Table 2: Oxygen binding energies E_{bind} at the different positions of the four-atom-wide step labeled in Figure 3a. All values are referenced to position E (see Figure 3c), where binding is most stable.

Binding site	E_{bind} [eV]	Binding site	E_{bind} [eV]
A	+0.54	E	0.00
B	+0.04	F	+0.64
C	+0.03	G	+0.42
D	+1.00	H	+0.63

diction to the TEM analysis, which again found a projected distance of Ag3 to its neighbor Ag5 (along direction 1) of 2.8 Å. Based on these results, the calculations were extended by adding a second oxygen atom per step-edge atom to the system. The most stable configuration is shown in Figure 3d, in which O1 is as discussed before and O2 now prefers position A. While the additional oxygen atom leaves the projected distance between Ag3 and Ag4 almost unchanged, the distance between Ag3 and Ag5 increases to 2.761 Å, in better agreement with the TEM analysis.

To better understand these observations, images of an Ag particle surface were simulated as a function of defocus and slab thickness. Simulated images clearly show the contrast variation perpendicular to the surface of the metal particles. Thus, the exact positions of the atoms in the terminating plane can be further corroborated. Figure 4 shows a high-resolution image (an enlarged part of Figure 2) together with an image along the [110] zone axis simulated by using the DFT-optimized structure with two oxygen atoms per unit cell (Figure 3d). The nearly perfect match between the experimental image and the simulations is obvious from Figure 4, that is, the Ag surface with subsurface oxygen atoms approximates the real surface structure of the studied Ag particles well. Simulated images also show that the elongated contrast variation of the terminating plane stretching into the vacuum is not an expression of a surface reconstruction, but the natural appearance of a terminating plane. When going from the surface towards the bulk in both the experimental

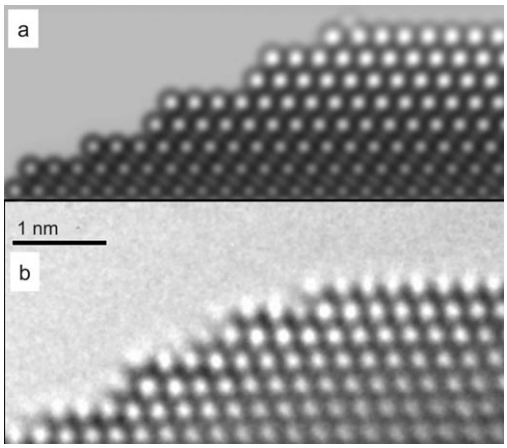

Figure 4. a) High-resolution image simulated by using the structure given in Figure 3d. b) An experimental image of such a termination.

and simulated images, the observed contrast variation of the Ag columns indicates the wedge-shaped structure of the metal particle. From the comparison between the calculations and the TEM analysis, we conclude that the presence of two oxygen atoms per step-edge atom is indeed capable of inducing the displacement of step-edge atom Ag3 that is observed experimentally. While O1, which forms a local oxide at the step, causes an increase in the projected distance of Ag3 along direction 3, O2 leads to an increase in distance along direction 1. Finally, although the distance increase along directions 1 and 3 could be explained for two oxygen atoms adsorbed on the step edges, a discrepancy still remains between the calculated and measured values for the outermost atom (located below the step edge) along direction 2. Since this is certainly caused by additional subsurface oxygen atoms, starting at the step edge, then diffusing into the step edge, and finally filling additional sites below the Ag surface layer, future calculations will aim at additional subsurface oxygen atoms as well as the barriers for oxygen diffusion along subsurface positions.

The surface and subsurface oxygen atoms found by Ertl et al.[1–3] are active sites for Ag catalysts in many oxidation reactions and have been the topic of both experimental and theoretical studies.[16–22] Experimentally, the surface and subsurface oxygen species have been studied by temperature-programmed desorption[16] and Raman,[17] IR,[16,18] and X-ray photoelectron spectroscopy,[19] but only after the silver catalyst was exposed to oxygen at high temperature. It is believed that oxygen pretreatment at high temperature results in the formation of subsurface oxygen and activates the catalyst.[16,17] However, it appears that the formation of subsurface oxygen and lattice oxygen is accompanied by a faceting of the silver surface.[23] While the driving force of the phenomenon (does subsurface oxygen diffusion result in the reconstruction of silver and therefore facet formation, or does facet formation lower the energy barriers for oxygen diffusion and therefore support the formation of subsurface oxygen?) remains an issue, our HRTEM and DFT study reveals that surface and subsurface oxygen atoms can be chemisorbed locally on Ag particles on the pre-existing steps, without high

temperature treatment in an oxidizing atmosphere. This could be the unique property of silver compared to other metals, for example, gold. Our HRTEM study on gold revealed no lattice expansion that could be related to local oxide formation (see Figure S2). No indication of oxygen in bulk silver can be extracted from our study. This may be due to the high barrier for oxygen diffusion into the bulk of silver, which can be overcome at high temperature. We note that theoretical works[20–22] mainly use a smooth silver (111) surface to study the effect of subsurface oxygen atoms on the reactivity of silver. Our DFT calculations were based on the HRTEM observations showing a more realistic silver surface consisting of steps and terraces (Figure 3a and c) and identified two distinct kinds of oxygen atoms, one adsorbed on the step edge and the other in the step edge (surface O2 and subsurface O1; Figure 3d).

According to our calculations, the binding energy of O2 on the surface is about 0.54 eV higher than the binding energy of O1 in the edge. It can thus be concluded that the desorption temperature of O2 is lower than that of O1. Therefore, the identified oxygen species can be related to the published TDS data[1–3,23] that identified surface oxygen atoms (O2) as those desorbing at lower temperature (<600 K), and subsurface oxygen atoms (O1) as those desorbing at high temperature (>900 K).

We have demonstrated that a combination of TEM corrected for spherical aberration with DFT calculations allows the investigation of the real atomic structure of Ag particles. Surface features such as terraces, steps, and edges can be clearly studied when the Fresnel fringes are eliminated by spherical-aberration correction. This makes the interpretation of the atomic surface structure of Ag particles straightforward. Based on the analysis of aberration-corrected high-resolution images and DFT calculations, we reveal for the first time that surface (α) and subsurface oxygen atoms (γ) are positioned on the edge and steps of Ag surfaces, while surface oxygen atoms on or under terraces with perfect lattice-plane termination seem energetically unfavorable.

Experimental Section

A 200-kV TEM (FEI Tecnai F20ST) equipped with a CEOS image spherical-aberration corrector was used. A combination of hexapole and octupole lenses producing negative spherical aberration was used to compensate the spherical aberration C_s of the objective lens.[9] The magnification of the system was calibrated on a standard gold sample. Details of the TEM experiments are given in the Supporting Information. High-resolution images were simulated with JEMS.[10] Simulations were carried out by the multislice approach with the theoretical parameters of the microscope and crystal structure as input. The catalyst was provided by TU Darmstadt, Germany. The synthesis was described elsewhere.[4] A brief summary of the preparation can be found in the Supporting Information.

All calculations were performed with SeqQuest,[11] a periodic DFT program using localized basis sets (double-zeta plus polarization level) represented by a linear combination of Gaussian functions and standard (nonlocal) norm-conserving pseudopotentials[12] with a nonlinear core correction.[13] As exchange-correlation functional we used the PBE[14] generalized gradient approximation (GGA). The different Ag(111) steps were modeled by slabs consisting of eleven layers with steps on both surface sides. The slabs were generated on the basis of the calculated bulk lattice constant of $a_0 = 4.136$ Å (experimental value at room temperature:[15] 4.09 Å). Due to the symmetry of the slabs, the entire system was allowed to fully optimize its geometry (to <0.01 eV Å^{-1}) in each calculation. Finally, integrations in the reciprocal space were performed with a converged Brillouin zone sampling of 132 k points per Å^{-1}.

Received: January 25, 2008
Revised: April 4, 2008
Published online: May 30, 2008

Keywords: density functional calculations · electron microscopy · oxygen · silver · surface chemistry

[1] X. Bao, M. Muhler, B. Pettinger, R. Schlögl, G. Ertl, *Catal. Lett.* **1993**, *22*, 215.
[2] X. Bao, M. Muhler, R. Schlögl, G. Ertl, *Catal. Lett.* **1995**, *32*, 185.
[3] H. Schubert, U. Tegtmeyer, D. Herein, X. Bao, M. Muhler, R. Schlögl, *Catal. Lett.* **1995**, *33*, 305.
[4] M. Bron, E. Kondratenko, A. Trunschke, P. Claus, *Z. Phys. Chem.* **2004**, *218*, 405.
[5] J. M. Thomas, P. L. Gai, *Adv. Catal.* **2004**, *48*, 174.
[6] P. L. Gai, E. Boyes, *Electron Microscopy in Heterogeneous Catalysis*, 1st ed., Institute of Physics Publishing, Bristol and Philadelphia, **2003**.
[7] L. D. Marks, D. J. Smith, *Nature* **1983**, *303*, 316.
[8] A. K. Datye, D. J. Smith, *Catal. Rev. Sci. Eng.* **1992**, *34*, 129.
[9] M. Haider, H. Rose, S. Uhlemann, B. Kabius, K. Urban, *J. Electron Microsc.* **1998**, *47*, 395.
[10] P. A. Stadelmann, *Ultramicroscopy* **1987**, *21*, 131.
[11] C. Verdozzi, P. A. Schultz, R. Q. Wu, A. H. Edwards, N. Kioussis, *Phys. Rev. B* **2002**, *66*, 125408.
[12] D. R. Hamann, *Phys. Rev. B* **1989**, *40*, 2980.
[13] S. G. Louie, S. Froyen, M. L. Cohen, *Phys. Rev. B* **1982**, *26*, 1738.
[14] J. P. Perdew, K. Burke, M. Ernzerhof, *Phys. Rev. Lett.* **1996**, *77*, 3865.
[15] C. Kittel, *Introduction to Solid State Physics*, Wiley, New York, **2004**.
[16] Z. Qu, M. Cheng, W. Huang, X. Bao, *J. Catal.* **2005**, *229*, 446.
[17] B. Pettinger, X. Bao, I. Wilcock, M. Muhler, R. Schlögl, G. Ertl, *Angew. Chem.* **1994**, *106*, 113; *Angew. Chem. Int. Ed. Engl.* **1994**, *33*, 85.
[18] Z. Qu, W. Huang, M. Cheng, X. Bao, *J. Phys. Chem. B* **2005**, *109*, 15842.
[19] M. Rocca, L. Vattuone, L. Savio, F. Buatier de Mongeot, U. Valbusa, G. Comelli, S. Lizzit, A. Baraldi, G. Paolucci, J. A. Groeneveld, E. J. Baerends, *Phys. Rev. B* **2001**, *63*, 081404(R).
[20] S. Linic, M. A. Barteau, *J. Am. Chem. Soc.* **2003**, *125*, 4034.
[21] W. Li, C. Stampfl, M. Scheffler, *Phys. Rev. Lett.* **2003**, *90*, 256102.
[22] Y. Wu, J. Greeley, M. Mavrikakis, *J. Am. Chem. Soc.* **2005**, *127*, 12823.
[23] A. J. Nagy, G. Mestl, D. Herein, G. Weinberg, E. Kitzelmann, R. Schlögl, *J. Catal.* **1999**, *182*, 417.

